ICARUS 113, 423–441 (1995)

Ice-on-Ice Impact Experiments

MANABU KATO AND YU-ICHI IIJIMA

Department of Earth and Planetary Sciences, Nagoya University, Nagoya 464-01 Japan
E-mail: kato@tomato.eps.nagoya-u.ac.jp

MASAHIKO ARAKAWA

Institute of Low-Temperature Science, Hokkaido University, Sapporo 060 Japan

YASUYUKI OKIMURA

Department of Earth and Planetary Sciences, Nagoya University, Nagoya 464-01, Japan

AKIO FUJIMURA

Institute of Space and Astronautical Science, Sagamihara 229, Japan

NORIKAZU MAENO

Institute of Low-Temperature Science, Hokkaido University, Sapporo 060, Japan

AND

HITOSHI MIZUTANI

Institute of Space and Astronautical Science, Sagamihara 229, Japan

Received February 16, 1993; revised September 23, 1994

Impact experiments, cratering and fragmentation, on water ice were performed in order to test the scaling laws previously constructed on rocks and sands for studying the collision process in the planetary history. The installation of a vertical gas gun in a cold room at −18°C (255 K) made it possible to use a projectile of water ice and to get the detailed mass distribution of ice fragments. Experimental results indicated the necessity for large modification of those scaling laws. Material dependence was investigated by using projectiles of ice, aluminum, and polycarbonate. Differences were observed in the morphology and efficiencies of cratering and in the energies required to initiate the fragmentation. Moreover, an abrupt increase of cratering efficiency, suggesting a change of excavation mechanism, was found at a critical diameter of spalled crater. The mass (size) distribution of small ice fragments obeyed a power law with an exponent significantly larger than that in rocks. The exponent was the same as that in Saturn's ring particles estimated from the data by the microwave occultation, which indicates a collisional disruption ring origin.

INTRODUCTION

Water ice was found to be one of most abundant minerals in the outer Solar System by the Voyager spaceprobes. The disruptive properties on the ice must be studied in order to make clear the formation process of outer planets and satellites. Some impact experiments on water ice were carried out after the Viking and Voyager missions (Croft *et al.* 1979, Croft 1981, Lange and Ahrens 1981, 1987, Kawakami *et al.* 1983, Cintala *et al.* 1985). However, their experimental results had a critical limitation in the comparison with those on rocks such as basalt and pyrophyllite due to insufficient collection of fragments. Moreover, they could not use a projectile of water ice in their experimental conditions. The dependence of crater shape on projectile materials was pointed out in employing projectiles of aluminum and polycarbonate (Kawakami *et al.* 1983). On the basis of experimental results on rocks and sands, scaling laws on cratering and fragmentation have been constructed to apply to the natural impact events (e.g., Hartmann 1969, Housen and Holsapple 1990, Mizutani *et al.* 1983, 1990). However, they must be tested by experiments on materials with a wide range of disruptive properties. Water ice was thought to be a suitable test piece for this purpose; the compressive strength of water ice is smaller than that of rocks by two orders of magnitude.

0019-1035/95 $6.00

We installed an impact gun facility in a cold room controlled at the temperature of −18°C for realizing the use of ice projectiles (for like-material collision) and the recovery of unmelted ice fragments. In this paper we describe the experimental procedure and results for cratering using sufficiently large targets to be considered "semiinfinite," and fragmentation using targets small enough to be disrupted catastrophically. Then we discuss the applicability of scaling laws by comparing with the experimental results obtained previously.

EXPERIMENTAL PROCEDURES

All experimental sequences except for monitoring the impact velocity and controlling the propellant gas were performed under low temperature: preparation of ice projectiles and targets, measurements of crater dimensions, and sieve-analysis of fragments. The cylindrical projectile, 1.7 g in weight, 15 mm in diameter and 10 mm long, of water ice was frozen in a metal mold from distilled water. The projectile consisted of irregular-shaped polycrystals with about 1-mm grain size. The projectile was colored with red ink to distinguish between the ejecta from the projectiles and targets. The dye effect on crater dimensions was checked before a series of present experiments were started. Projectiles of polycarbonate (2.0 g), aluminum alloy (JIS A5052, 5.0 g), and basalt (from Chausuyama, Japan; 5.2 g) with the same size as the ice were also employed for comparing the dependence of disruptive effects on projectile material. Two kinds of ice targets were used; a fine-grained ice block (hereafter called Ice F), consolidated from a mixture of ground snow powder and a small amount of cooled water (a few percent volume ratio), and a commercial ice block (hereafter Ice C), which consisted of large elongated ice crystals. Although Ice F was non transparent due to the porosity of 1%, constituent grains were fine and homogeneous (Fig. 1a) due to slow freezing in one direction for 1 week in the cold room. Transparent Ice C was always hit in the direction of crystal elongation (Fig. 1b), i.e., *a* axis. The Ice C blocks were quarried out to avoid a weak cloudy zone in the center of an original block of dimensions 1 × 0.6 × 0.35 m.

Target sizes were selected corresponding to the experimental purpose and impact velocity: from 30-cm^3 to 50 × 50 × 35-cm rectangular solid for cratering, and cubes with edge lengths of 5 to 10 cm for fragmentation experiments. In cratering experiments Lange and Ahrens (1987, for ice) and Polanskey and Ahrens (1990, for gabbro) confined the target in hard pipes to make a crater without any split of side edge of the target block. In the present experiment a larger ice block of 30 to 50 cm in size was used to prohibit any disruptive radial fractures reaching the flank of target, and the formation of cracks originating at the edge of the block in unconfined targets. In the fragmentation experiment target blocks were set on a polyurethane form sheet of 10 cm thick in a recovery box of 40 cm^3 to approximate a free surface condition. The inner walls of the box were covered by 5 cm thick polyeretane sheets to prevent fragments from being refragmented on the walls in the same manner as Kawakami *et al.* (1983) and Takagi *et al.* (1984).

A vertical gas gun was installed in the cold room at the Institute of Low-Temperature Science of Hokkaido University, in which the room temperature was kept at a constant temperature of −18°C. Two kinds of propellant high-pressure gas were employed corresponding to desired velocity range: N_2 gas for velocity lower than 300 m/s and He for that from 300 m/s to 1 km/s. The gun was fired by breaking a metal diaphragm with a pin for N_2 shots, and by reducing the gas pressure in a subsidiary chamber attached between the gun barrel and the breech for the high-pressure He. About 10 MPa of He gas was required to accelerate the 1.7-g ice projectile to a velocity of 1 km/s. An evacuated steel target chamber about 80 cm in diameter with some view ports was standing below the gun barrel. The impact velocity was measured by the conventional method of recording the flight time difference of projectile between two laser beams using a digitizing oscilloscope. We worried about fragmentation or melting of projectiles in firing the physically weak ice before this experiment being started. However it was found that no special techniques were necessary in our experimental range by monitoring the oscilloscope and by checking the recovered ice targets. Sometimes we observed signals of more than two on the oscilloscope and noncircular craters with plural dyed central pits. Those data were discarded in this study. High-speed cinematography also demonstrated the projectile integrity. The ice projectile was accelerated by about 20% more efficiently the other materials, probably due to the lower friction of ice.

Impact fragments were collected with a recovery rate of more than 97% for determining the mass distribution and the volume of craters. The mass of fragments was also measured in the cold room using hand-picking and sieve analysis to the order of 10^{-5} g.

RESULTS AND DISCUSSIONS

Cratering Experiments

Experimental conditions and results of the cratering experiments are summarized in Table I. The peak pressure generated in collision P_0 was estimated by the planer impact approximation (Melosh 1989) using the Hugoniot of ice compiled by Gaffney (1985, 1973, Larson 1984), ignoring temperature difference between the present study (255 K) and the Hugoniot data (263 K). The late stage effective energy E_{LS} (P_0 multiplied by a projectile volume), introduced as a suitable scaling parameter in

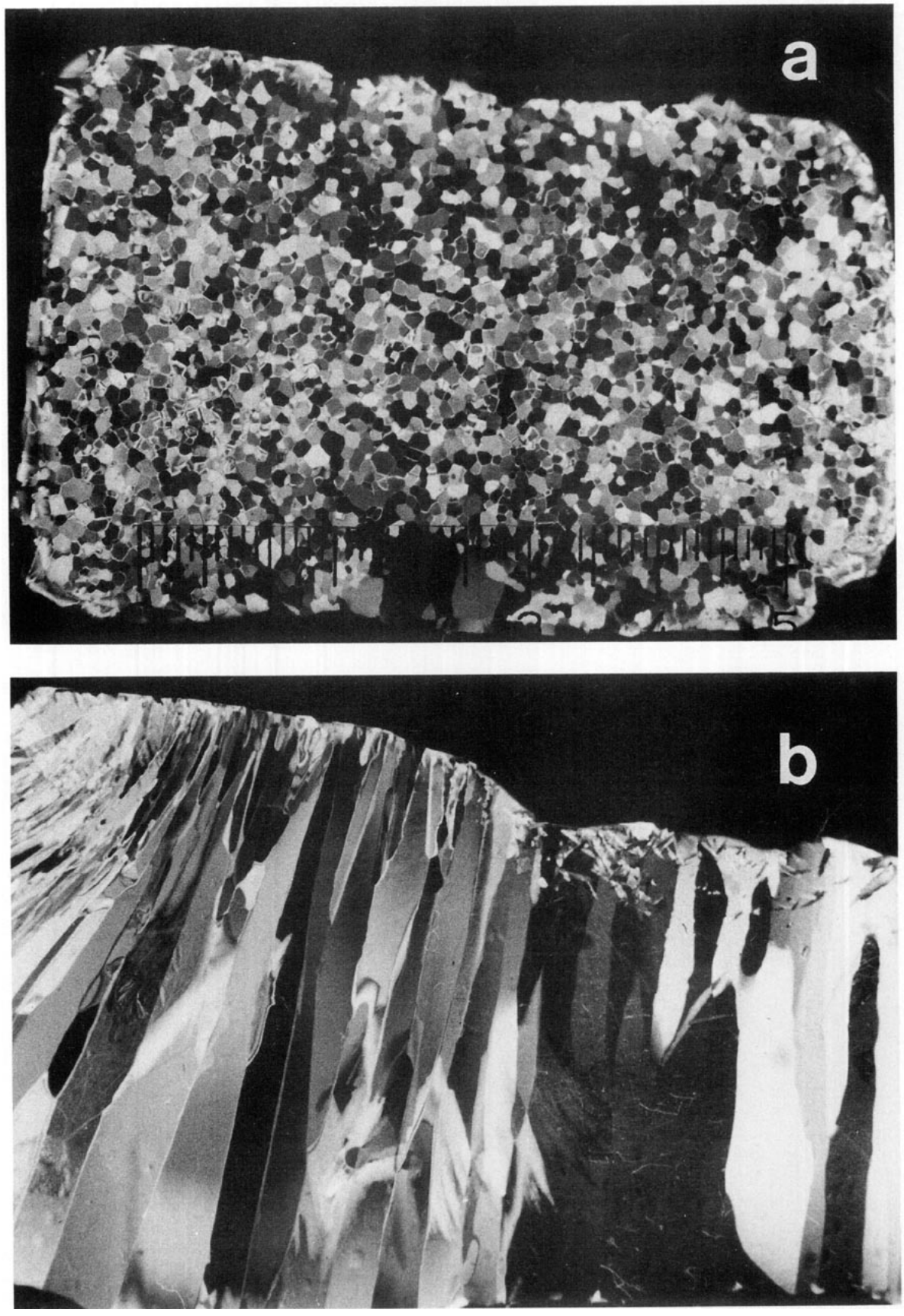

FIG. 1. Polarized photomicrographs of (a) Ice F, and (b) Ice C. Both (a) and (b) are the same scale. The scale indicates 1 mm of length.

TABLE I
Experimental Conditions and Results of Cratering on Ice

Run No.	V_i m/s	E_k J	E_{LS} J	P_0 MPa	Pit dia. cm	Spall dia. cm	Outer sp. dia. cm	Pit depth cm	Crater volume cm^3	Crater type
IF1	83	6	247	140	(1.5)	1.50	4.3	0.19	0.4	tab.plat.
IF2	152	20	424	240	(2.2)	2.52	5.5	0.33	1.7	tab.plat.
IF3	253	54	530	300	(2.9)	3.50	8.7	0.49	3.4	tab.plat.
IF4	299	76	636	360	(3.3)	4.80	10.	0.69	11.4	tab.plat.
IF5	330	94	707	400	3.4	5.70	9.3	1.23(0.86)	29.5	pit
IF6	371	117	795	450	2.5	6.84	12.6	1.37(1.06)	38.2	pit
IF7	397	134	848	480	2.3	7.41	13.1	1.81(1.28)	61.5	pit
IC0	36	1	106	60						intact
IC1	116	11	345	195	(1.59)	2.36	4.3	0.24	0.7	tab.plat.
IC2	174	26	495	280	-	3.01	4.5	0.29	1.6	tab.plat.
IC3	246	51	530	300	(2.3)	3.26	6.2	0.47	2.2	tab.plat.
IC4	299	76	636	360	(3.7)	3.99	7.4	0.45	4.7	tab.plat.
IC5	355	108	724	410	3.24	7.08	8.9	1.79(0.96)	54.1	pit
IC6	372	118	742	420	3.53	7.33	16.0	1.93(0.74)	55.8	pit
IC7	388	128	760	430	2.29	8.71	15.6	2.86(1.24)	104.2	pit
IC8	460	180	839	475	4.74	10.7	24.0	2.0(0.9)	92.0	pit
IC9	607	313	990	560	3.52	11.9	28.5	5.1(1.4)	140.0	pit
IC10	807	554	1201	680	3.60	18.9	30.0	5.95(2.46)	496.3	pit
PC1	106	12	309	175	-	3.2	4.8	0.62	3.9	tab.plat.
PC2	160	26	459	260	-	4.1	8.4	0.75	5.5	tab.plat.
PC3	227	52	557	315	-	6.1	8.6	0.98(0.78)	15.9	tab.plat.
PC4	279	78	698	395	-	7.3	11.2	1.44(1.06)	30.0	tab.plat.
PC5	315	99	760	430	(1.47)	9.8	15.9	1.74(1.06)	56.5	tab.plat.
PC6	349	129	813	460	-	10.4	13.2	1.88(0.94)	60.0	tab.plat.
AC1	62	10	300	170	-	3.4	3.9	0.5	-	tab.plat.
AC2	73	13	336	190	-	4.1	6.0	0.72	5.8	tab.plat.
AC3	109	30	512	290	-	4.95	8.5	1.09(0.6)	11.8	bowl with cp
AC4	176	77	654	370	-	6.4	10.0	1.50(1.21)	30.0	bowl with cp
AC5	227	129	795	450	-	9.6	11.1	2.20(1.16)	95.2	bowl with tp
AC6	250	156	813	460	-	11.4	18.2	2.18(1.80)	132.6	bowl with cp
AC7	290	210	901	510	5.4	13.1	14.4	2.76(1.87)	216.0	bowl with ff
BC1	59	9	283	160	-	3.1	4.4	0.8	2.2	bowl
BC2	208	110	760	430	-	7.5	10.8	1.5	29.9	bowl
BC3	228	127	795	450	-	7.4	10.4	2.35	43.4	bowl
BC4	256	174	830	470	5.6	11.2	12.4	2.7(1.7)	96.4	double bowl
BC5	277	198	875	495	6.1	13.1	18.1	2.8(1.8)	132.9	double bowl

Symbols of run numbers indicate the sets of projectile and target materials. IF, ice and Ice F; IC, ice and Ice C; PC, polycarbonate and Ice C; AC, aluminum and Ice C; BC, basalt and Ice C. Numbers in parentheses in the column of pit depth show the depth of double crater. In the abbreviation of crater type tab.plat.(tp) is tabular plateau; cp, central peak; ff, flat floor.

Mizutani *et al.* (1983, 1990), was calculated. Measured sizes and morphologies of craters are also described in the table.

(1) Crater shape and morphology. Three general types of craters were formed depending on the impact velocity and projectile materials: a pit type for high-energy ice projectiles; tabular plateau-type craters in the low-energy ranges by ice, polycarbonate, and aluminum projectiles; and bowl type for aluminum alloy and basalt projectiles in the range of high-impact energy. Schematic illustrations are given in Fig. 3, in which predominant differences are found in the shapes of rims surrounding the central tables for tabular plateau-type craters of Fig. 3b (Run IF4) and Fig. 3c (PC3) and in the details in the central region for bowl-type craters (a central pit (Fig. 3a, IC7), a central peak (Fig. 3d, AC4), a tabular plateau (Fig. 3e, AC5), a flat floor (Fig. 3f, AC7), or a simple double (Fig. 3g, BC4)). Two example photographs of cross-sectioned craters are presented in Fig. 4 for Run IC7 and Run AC5. These cratered targets were kept in the cold room for 1 month to make large cracks conspicuous by healing fine cracks. During this time the crater's sharp edges and rims disappeared due to sublimation of ice, although crater shapes and sizes were preserved. Figure 4a shows a pit-type crater made by an ice projectile, while Fig. 4b shows a bowl-type crater made by an aluminum alloy projectile. This difference of crater shape in spite of the same conditions of impact energy (E_k, E_{LS}) and P_0 also reflects in the formation of the fracture pattern: preferential growth of down-going fractures from the bottom of crater pit in Fig. 4a and homogeneous extension of radial fractures in Fig. 4b. This difference, which must be related to differences in the projectile material is not yet clearly explained. However, we think that it is closely related to the breakage of the ice projectile. The impact pressure exceeded the strength of the ice projectile, so the projectile was completely disrupted by the impact. Figure 2b shows that the dyed projectile was broken in pieces smaller than 1 mm even at low impact velocity of 152 m/s. On the other hand, aluminum and basalt projectiles were kept intact and polycarbonate ones received only slight plastic deformation. Therefore, we conclude that an edge effect of a projectile must be manifested in the morphology of the crater.

Croft *et al.* (1979) shows an effect of impact directions, parallel or perpendicular to the long axes of ice grains, on details of crater morphology. They reported shallow square craters were made by the impact perpendicular to grain axis of "temperate ice." Considering this experimental result we planned to employ two types of ice blocks with significantly different grain sizes. However, significant differences between using Ice F and Ice C were not found either in crater morphology or in crater dimensions as discussed in the next section. Thin sectional examinations of recovered targets revealed that the cracks did not extend along the boundary of large grains, but traversed the boundary as if they ignored the existence of the boundaries. This fact implied there exists little effect of grain boundary and impact direction on impact fracture. We think that the difference between the present study and that of Croft *et al.* (1979), where square craters were apparently generated by grain boundary fracture, was the temperature effect. The gain boundary of temperate ice probably weakened for the temperature condition near melting point of ice.

(2) Crater dimensions. The definition for measuring sizes of crater are also given in Fig. 3 following Kawakami *et al.* (1983). Pit diameter indicates the diameter of a moat in the tabular plateau-type, central pit in pit-type, central flat floor in Run AC7, and central bowl in the double bowl-type craters. Spall diameter is the distance from edge to edge of the excavated crater. Outer spall diameter is measured as the diameter of cracks reaching to the upper

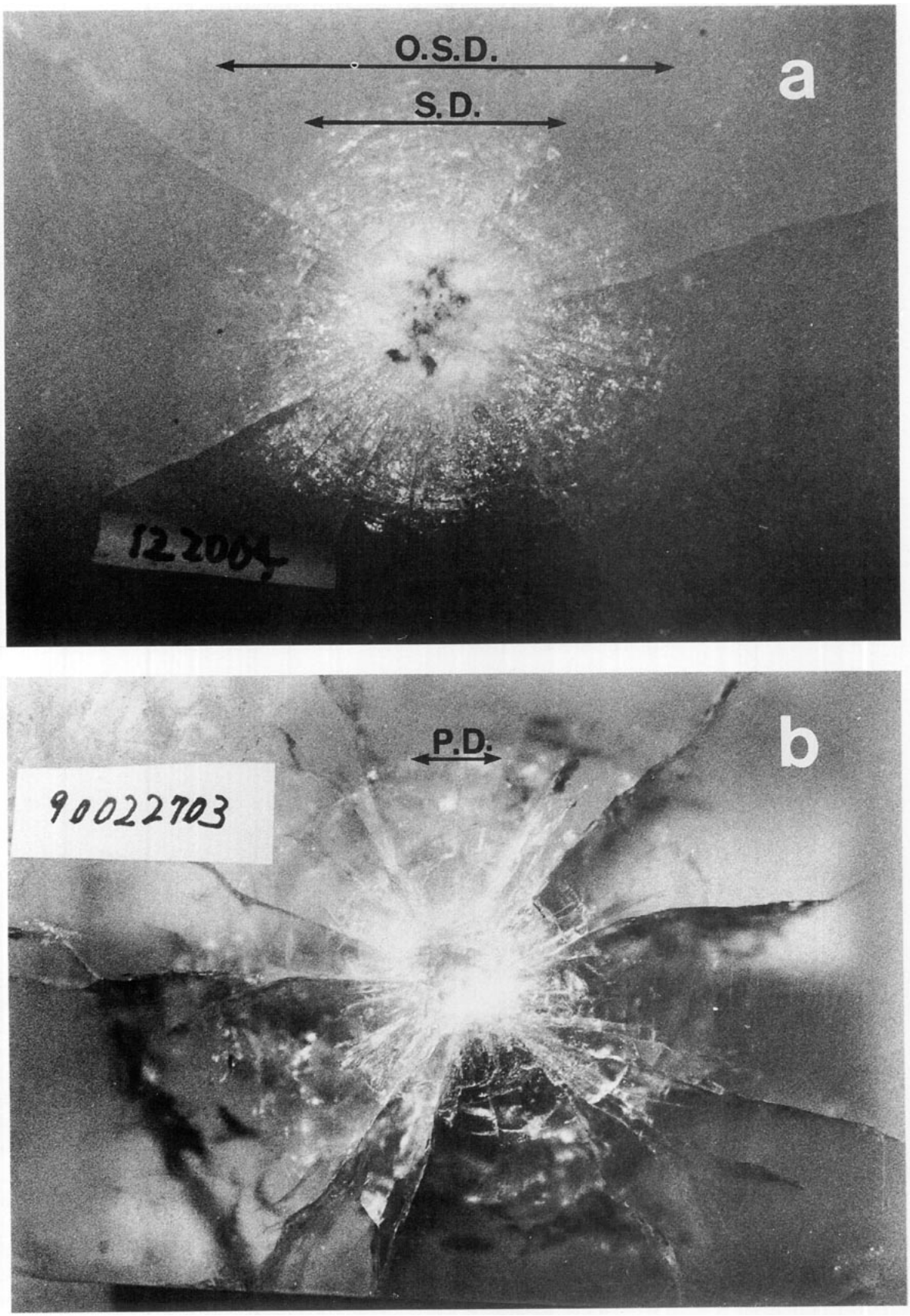

FIG. 2. Top views of craters for (a) Run IF2 and (b) IC6. Fragments of ice projectile colored by a red ink was observed in low-velocity impact of Run IF2.

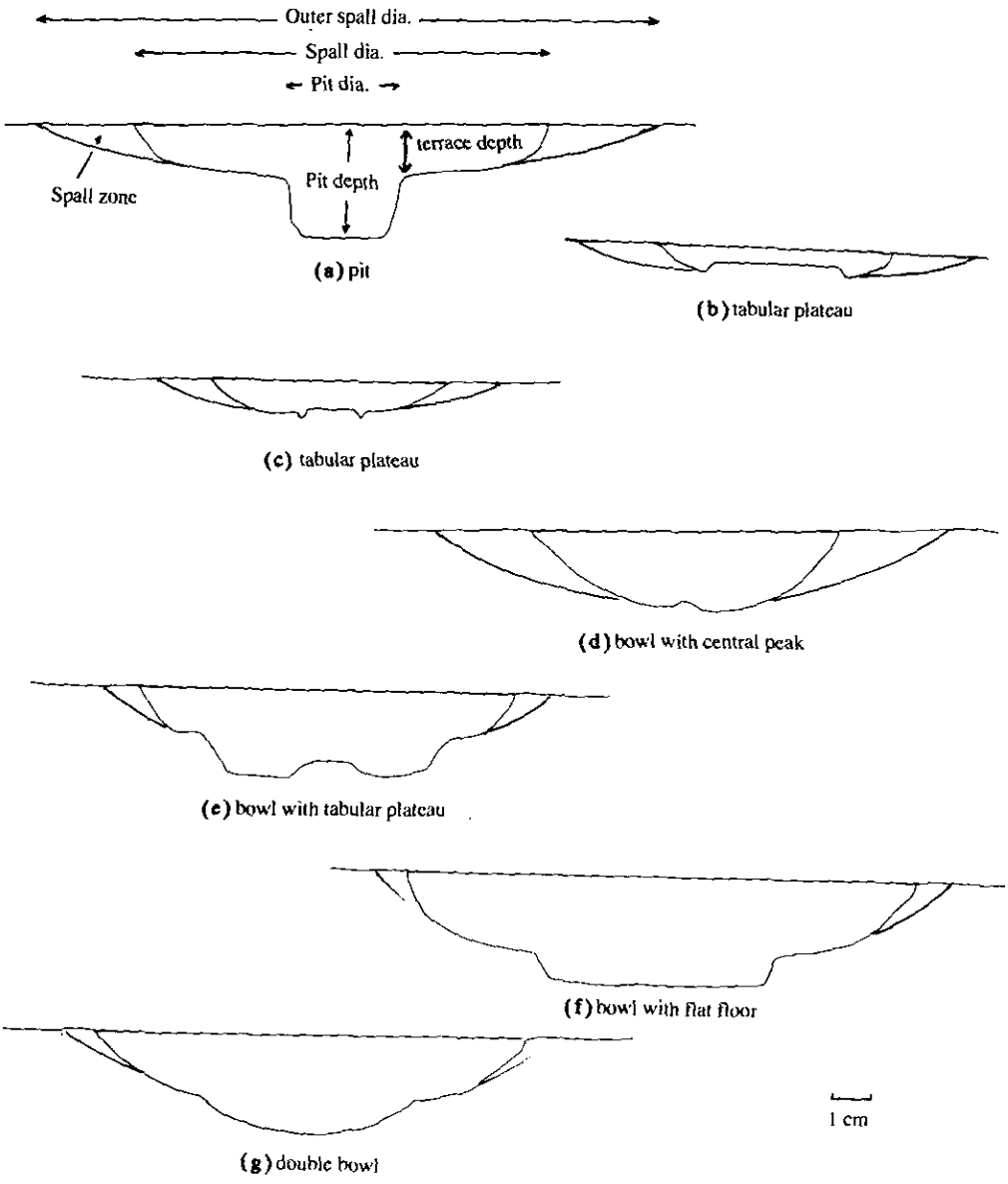

FIG. 3. Schematic cross sections of ice craters in Runs of (a) IC7, (b) IF4, (c) PC3, (d) AC4, (e) AC5, (f) AC7, and (g) BC4.

surface of target, leading to concentric spall fracture as shown in Fig. 2. Pit depth shows the maximum depth of terrace (in parentheses) and central pit for pit-type craters and the maximum depth and depth to the top of tabular plateau (in parenthesis) for tabular plateau-type craters. Crater volume was estimated by the ejecta mass and/or the geometry of crater.

The relations of the crater (spall) diameter and the crater volume against the projectile kinetic energy are presented in Figs. 5 and 6 comparing with the previous data by Croft *et al.* (1979), Kawakami *et al.* (1983), and Lange and Ahrens (1987). It can be seen that (1) the relation predominantly depends on the selection of projectile materials, especially in the low-energy range, and (2) the cratering efficiency abruptly increased from a certain value of impact energy (about 50 joules) for the ice projectiles. In the range lower than 50 joules, aluminum projectiles made larger craters than the ice projectiles by an order of magnitude in volume. No significant difference between Ice F and Ice C targets impacted by ice projectiles was found in the entire range of impact conditions studied, although the radial cracks in the case of Ice C target extended much farther than in the case of Ice F; the maximum length in Ice C was about 1.5 times that in Ice F.

In the high-energy range, the dependence of crater dimensions on the projectile material diminished, and our experiments well reproduced the results of Lange and Ahrens (1987) using 257 K unconfined targets. Kawakami

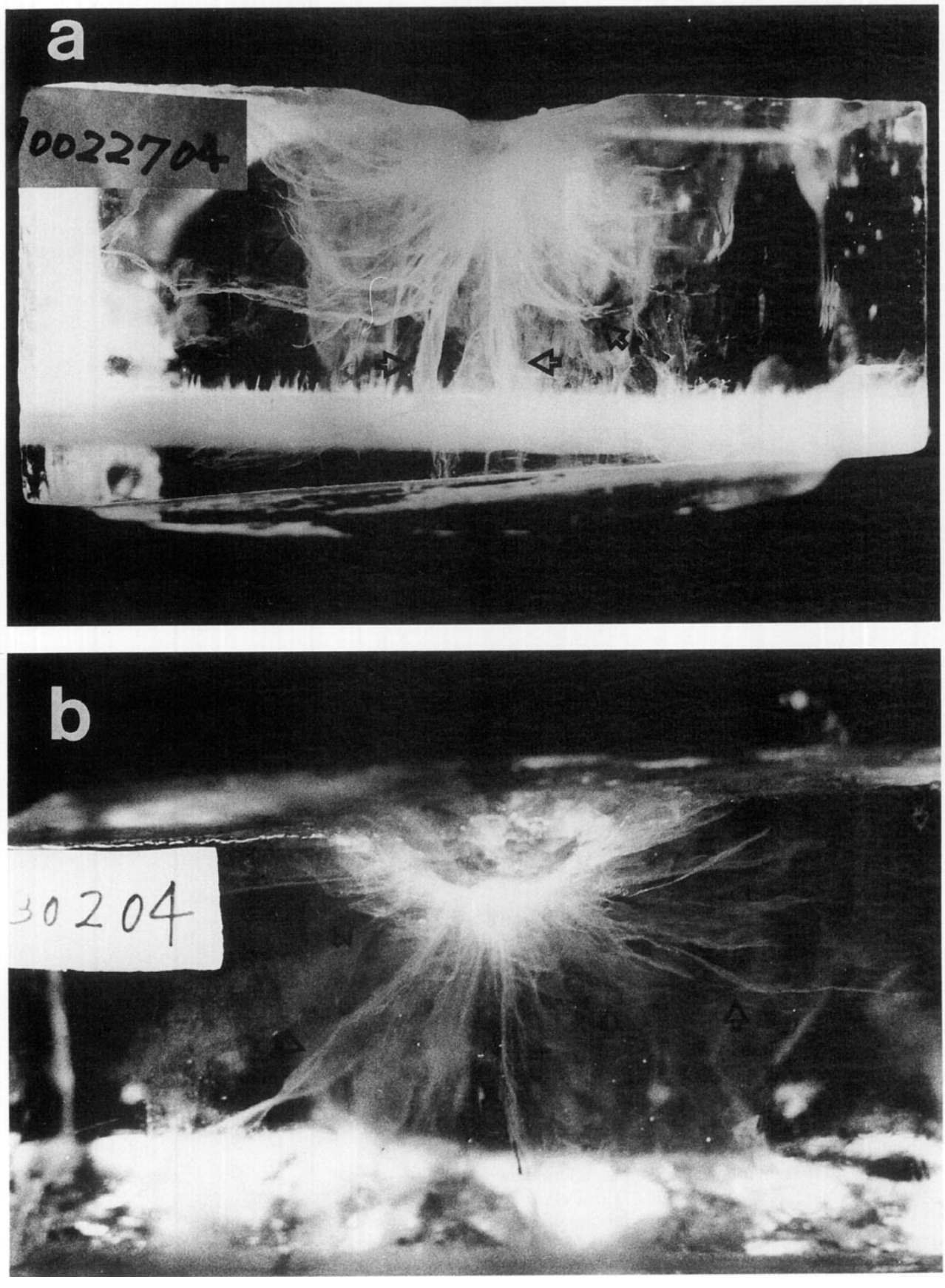

FIG. 4. Photographs of bisected ice craters in Runs of (a) IC7 and (b) AC4 after healing fine cracks. Arrows indicate characteristic fractures extended from the bottom of each crater.

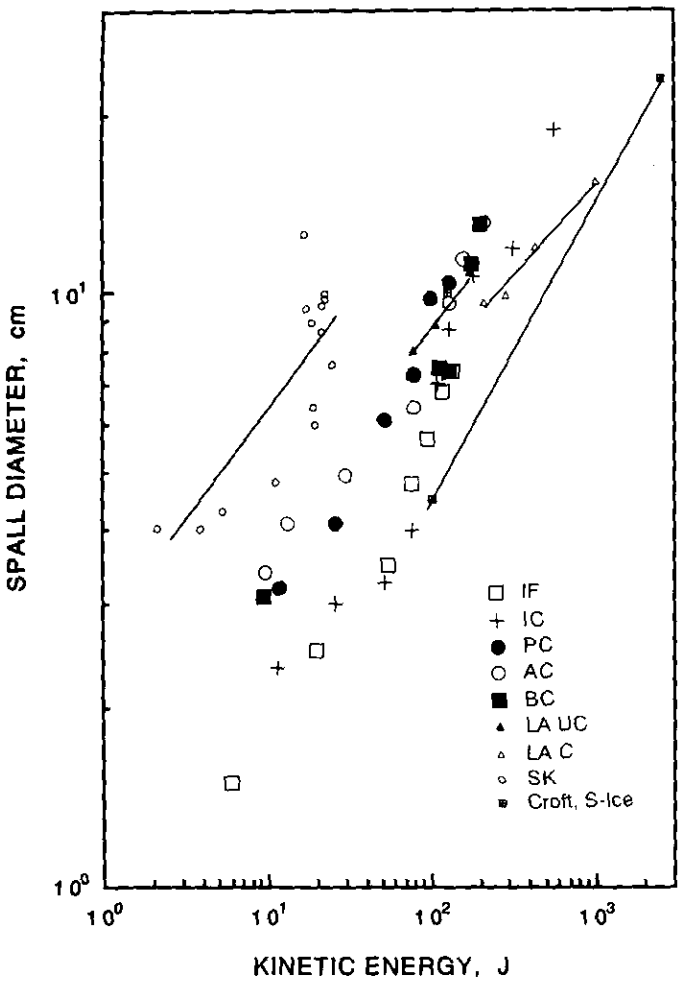

FIG. 5. Relation of spall diameter of ice craters versus projectile kinetic energy. Symbols represent the sets of projectile and target materials. IF, ice and Ice F; IC, ice and Ice C; PC, polycarbonate and Ice C; AC, aluminum and Ice C; BC, basalt and Ice C. The data and regression lines of previous studies (LA UC(unconfined) and LA C(confined), Lange and Ahrens 1987; SK, Kawakami *et al.* 1983; Croft, S-Ice; Croft *et al.* 1979) are also presented for comparison.

et al. (1983) have reported the results over a wide range of energy (three orders of magnitude). However, their data at high energy were obtained for ice targets exposed to ambient temperature. Moreover, their data even in the low-energy range to 40 joules showed large scatter. The spall diameters of twice those of the present results were also inconsistent with those of temperate ice in Croft *et al.* (1979) in spite of their very close temperature conditions. Kawakami *et al.* (1983) maintained the surface temperature (270 K) of ice blocks by sublimation of ice in vacuum. As discussed by Lange and Ahrens (1987), we cannot rule out yet the possibility of differences in sample preparation or temperature control method. The use of the cold room in this study eliminated the ambiguity in temperature control of ice targets. On the other hand, Lange and Ahrens (1987) employed "hard" ice by confining targets to form craters in small ice targets without splitting even at energies up to 10^3 joules. Their confinement reduced crater diameters to 2/3 those of ours at the same impact energy of a few hundred joules. The data from supercooled ice (S-ice) by Croft *et al.* (1979) also indicates the usage of "hard ice" frozen to about −70 C.

Figs. 5 and 6 suggested that it is necessary to fit our data by a regression line with an inflection for each combination of projectile and target, although previous cratering data using competent rocks including ice have been fit by a single straight line. Table II shows the coefficients a and power-law exponents b in the least-squares fitting for the crater diameter versus the kinetic energy and the crater volume versus the kinetic energy depending on the projectile materials and the impact energy ranges. Our fits have an inflection with a change in exponent b from 0.08 smaller than Kawakami *et al.* (1983) in the low-energy range to 0.65 larger than that of Lange and Ahrens (1987) in a high-energy one. Figure 5 suggests that IC targets possibly bend over at 200 J with a slope approximate to that of S-ice in Croft *et al.* (Croft, personal communica-

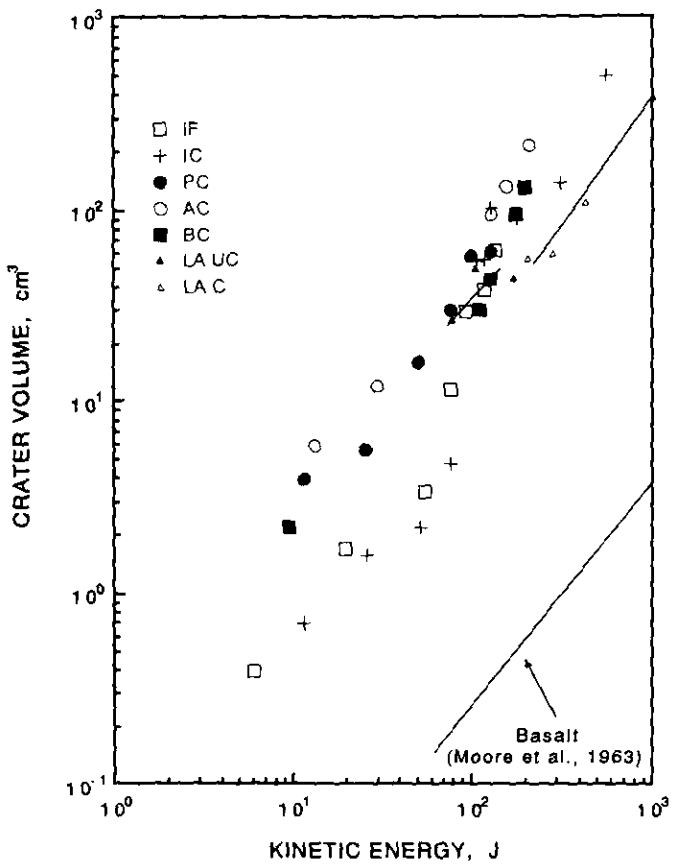

FIG. 6. Crater volume versus projectile kinetic energy for impact in this study, 257 K unconfined and confined ice, and basalt (Lange and Ahrens 1987, Moore *et al.* 1963).

TABLE II
Least-Squares Fitting in the Crater Diameter and Volume Versus Projectile Kinetic Energy

Projectile	$\log D\,(cm) = a_D + b_D \log E_k(J)$				$\log V\,(cm^3) = a_V + b_V \log E_k(J)$			
	$E_k < 50$ J		$E_k > 50$ J		$E_k < 50$ J		$E_k > 50$ J	
	a_D	b_D	a_D	b_D	a_V	b_V	a_V	b_V
Ice	-0.04	0.34	-0.50	0.68	-1.08	0.91	-1.55	1.55
PC	0.17	0.31	-0.23	0.60	-0.46	0.93	-1.44	1.55
Al	0.27	0.29	-0.32	0.62	-0.28	0.93	-1.56	1.68
Basalt			-1.27	1.03			-3.74	2.54
Al*1	0.45	0.37						
PC*2			0.15	0.38				
PC*3			0.23	0.31			-1.26	1.32
Lead*4			-0.054	0.4				

* 1, data from Kawakami *et al.* (1983); * 2, "unconfined" from Lange and Ahrens (1987); * 3, "confined" from Lange and Ahrens (1987); * 4, data from Croft *et al.* (1979).

tion). In order to solve this problem we need to use ice blocks larger than 50 cm limited by the dimension of present target chamber. Figure 6 also shows that the slope of ice data in low energy is close to that of competent basalt (Moore *et al.* 1963), although the volume of ice crater is larger than that of basalt by 1.5 orders of magnitude. This fact seems to be very suggestive, when the difference of material strength between ice and rock is considered. However, we cannot give yet any suitable explanation for inflections in the high-energy range of ice impacts.

In the following we describe the data sets using the "late-stage effective energy" E_{LS} proposed by Mizutani *et al.* (1983, Eq. (16), 1990) as a scaling parameter for strength-dominated cratering events,

$$E_{LS} = \frac{1}{2} mv \left(C_0 + \frac{1}{2} sv \right) = P_0 V_P,$$

where m, v, and V_P are projectile mass, velocity, and volume, respectively and C_0 and s are material parameters relating the shock velocity to particle velocity in the ice target. The relations of the spall diameter D_S versus E_{LS} and the excavated crater volume versus E_{LS} are presented in Figs. 7 and 8, respectively. The pit diameter versus E_{LS} by Kawakami *et al.* (1983) and the rim to rim distance of crater, namely spall diameter in the present study, versus E_{LS} by Lange and Ahrens (1987) are also given in the figures. The E_{LS} by Lange and Ahrens were recalculated here using the real Hugoniot of Gaffney (1985) suitable to these low-velocity impacts, although they were originally estimated using the Hugoniot by Ahrens and O'Keefe (1985). Kawakami *et al.* (1983) found a single power-law exponent 2/5 in the relation of the pit diameter with the energy without any use of scattered data of the spall diameter. However, it is impossible to identify the pit diameter by Kawakami *et al.* (1983) in the present crater morphology of double craters and single bowls. Therefore, we adopt the spall diameter and excavated volume for representative crater dimensions, as did Lange and Ahrens (1987). The data plotted have the same tendency as those in Figs. 5 and 6, an evident dependence of cratering on the projectile material in the low-energy range and an inflection of the regression lines at a critical value of energy, which corresponds to the drastic change of crater shapes. Table III shows the results of least-squares fittings in the log–log space. Using the ice projectiles in the low-energy range, the power-law exponent of b of 1.2 was obtained, while the value of b increased to 2.2 in the higher energy of impacts. The value b for basalt projectiles was markedly larger than for other kinds of projectiles like in the regression analysis on the crater dimension and the impact kinetic energy. The reestimated data of Lange and Ahrens (1987) were apart from the trends of present study in spite of b values close to those of present results in the low-velocity impacts.

Our data sets of experimental results are also adopted to

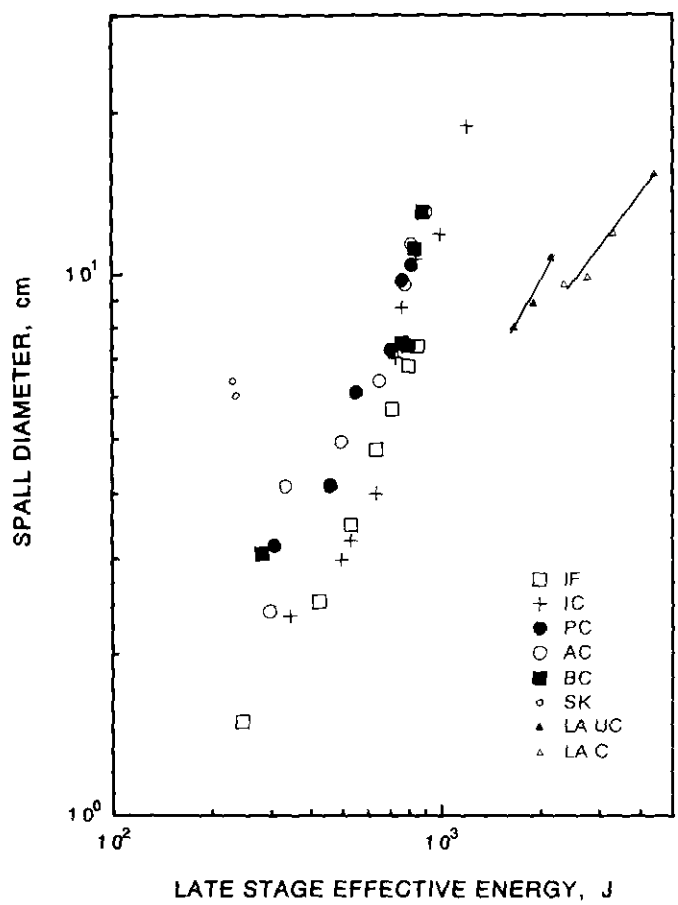

FIG. 7. Spall diameter versus late-stage effective energy (Mizutani *et al.* 1983, Kawakami *et al.* 1983).

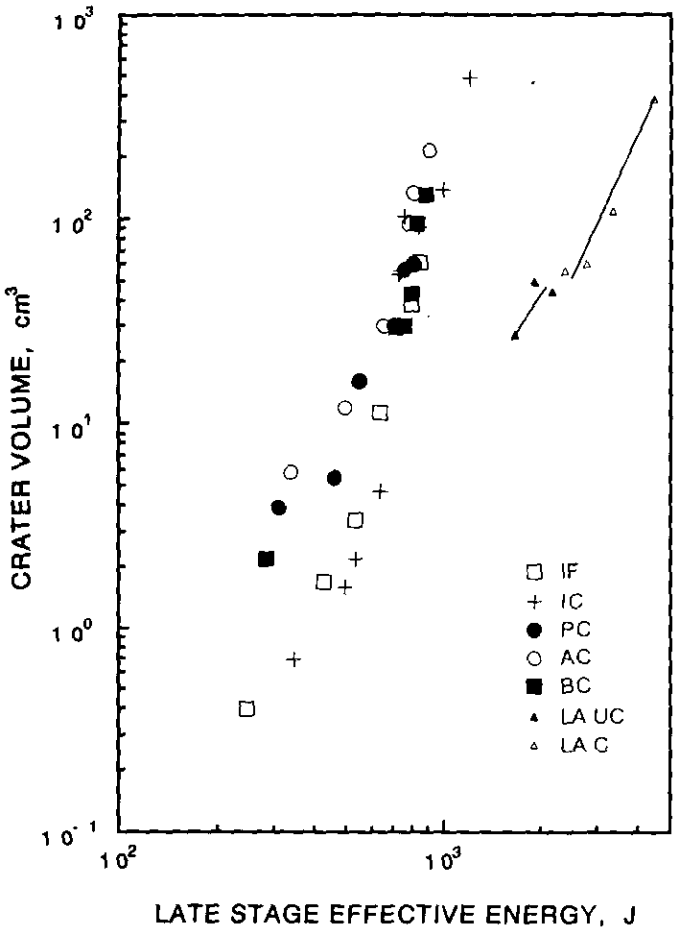

FIG. 8. Crater volume as a function of late-stage effective energy.

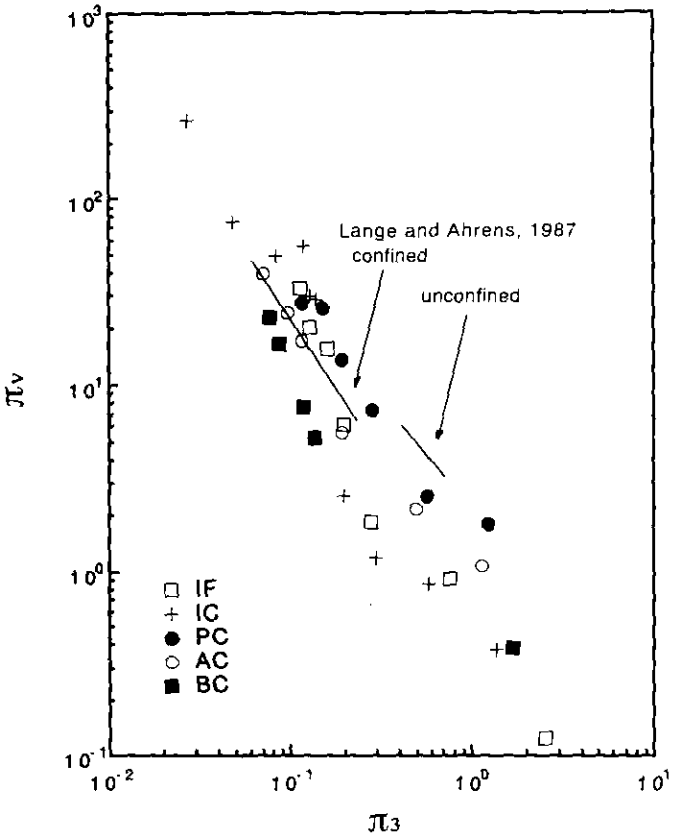

FIG. 9. π_V versus π_3 in the π scaling. The data of 257 K ice target (Lange and Ahrens 1987) are referred.

the similarity variable analysis, nondimensional π scaling defined by Holsapple and Schmidt (1982). The relation of scaled crater volume π_v versus π_3 is represented in Fig. 9, and the results of the regression analysis is given in Table IV. Figure 9 also shows the dependence of projectile material like above plottings by using the projectile kinetic energy and the late-stage effective energy. The data of confined ice targets by Lange and Ahrens (1987) can be plotted in a group of present data points, while the data from unconfined target are deviated a little from the present data despite the similar condition of ice target employed. The power-law exponents α on π_3 are equal to b

TABLE III
Least-Squares Fitting in the Crater Diameter and Volume Versus the Late Stage Effective Energy

Projectile	$\log D\,(cm) = a_D + b_D \log E_{LS}(J)$				$\log V\,(cm^3) = a_V + b_V \log E_{LS}(J)$			
	a_D	b_D	a_D	b_D	a_V	b_V	a_V	b_V
	$E_{LS} < 650$ J		$E_{LS} > 650$ J		$E_{LS} < 650$ J		$E_{LS} > 650$ J	
Ice	-2.7	1.2	-5.4	2.2	-7.8	3.1	-15.4	5.9
PC			-3.6	1.6			-10.3	4.2
Al	-2.1	1.0	-5.6	2.3	-5.3	2.4	-16.1	6.2
Basalt			-12.0	4.5			-30.9	11.2
PC*1			-2.8	1.2				
PC*2			-1.7	0.8				

* 1, "unconfined" 257 K ice; * 2, "confined" 257 K ice recalculated from the data of Lange and Ahrens (1987).

TABLE IV
Least-Squares Fitting in π Scaling

	$\pi_V\,\pi_3{}^{\alpha} = C_V$			
Projectile	$\pi_3 > 0.2$		$\pi_3 < 0.2$	
	C_V	α	C_V	α
Ice	0.53	0.91	1.01	1.55
PC	1.95	0.94	1.01	1.56
Al	1.19	0.93	0.43	1.68
Basalt			0.03	2.53
PC*1	3.19	0.55		
PC*2			1.04	1.32

π_V, $V\rho/m_P$, π_3, $Y/(2E_k/V_P)$.
* 1, "unconfined"; * 2, "confined" from Lange and Ahrens (1987).

of power-law exponents on E_k, by the definition of π_3. Therefore, the value of α and C_v by the least-squares fitting are largely different from the values by Lange and Ahrens (1987) as shown in Table IV.

Concerning the dependence of crater diameter on projectile material, we think that it originated from the difference of efficiency in partitioning the impact energy, probably due to destruction or deformation of ice or polycarbonate projectiles. So we reconsider the projectile volume V_P, the volume representative of isobaric core of the impact pressure P_0, in estimating E_{LS} or the inclusion of a factor smaller than 1.0 in E_k. When 0.6 V_P was applied as the effective volume, the trends of ice and aluminum projectiles agreed very much in the lower range of E_{LS}. This fact will be experimentally supported by the detection of impact duration. The discrepancy in the log D versus log E_{LS} between the data of "unconfined ice" by Lange and Ahrens, Kawakami *et al.*, and this study probably originated from the usage of different size of projectiles: 20 mm in diameter by Lange and Ahrens and 10 mm by Kawakami *et al.* The inconsistency was probably also improved by suitable estimation of the effective volume, namely the isobaric core. As to the inflection in the relation of D_s versus E_{LS} or E_k, it could be attributed to the melting or high-pressure phase change by impact. However, those increases of slope cannot be supported by previous experimental and theoretical studies. Possible high-pressure phases (ices III, IV, and V) are supposed to be limited only to the small portion of the target near the impact point. It could be possible to eliminate the inflection in D_s versus E_{LS} by reestimation of initially generated pressure P_0. In this study we used the Hugoniot at 263 K compiled by Gaffney (1985) neglecting temperature difference from our condition of 255 K. However, the temperature effect on Hugoniot of ice in these temperature conditions is expected to be very large considering the stable pressure range of Ice III or liquid phases.

The relation of crater diameter to depth is also presented in Fig. 10, which shows a ratio 0.2 of depth/diameter in the range of spall diameter smaller than 7 cm. The ratio increased to 0.3 in the larger diameter as corresponding to the morphological change of simple tabular plateau to double craters. These ratios, smaller than 0.5 of Croft *et al.* (1979), were presumably due to material difference of projectiles. We would like to try lead projectiles as used in Croft *et al.* (1979); however, our present facility is not powerful enough to fire heavy lead projectiles.

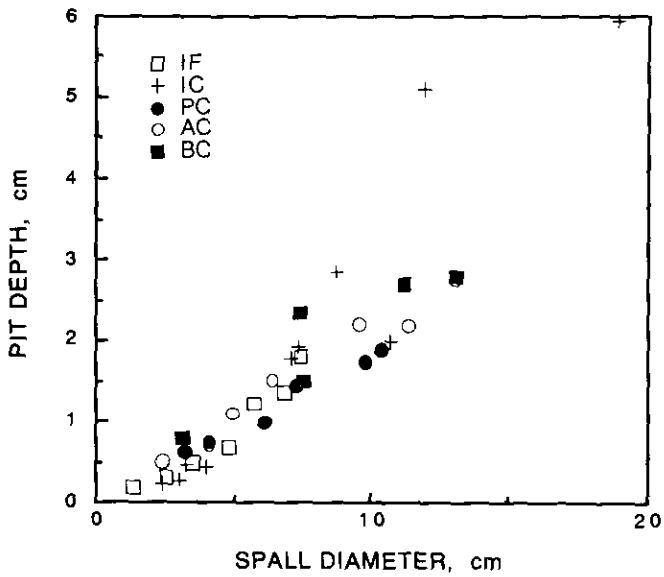

FIG. 10. Relation of pit depth with spall diameter of ice crater.

Fragmentation Experiments

In the following we show the results of fragmentation experiments using ice targets, referring to the previous fragmentation on the ice and rocks. One of the purposes of installing the experimental device in the cold room was to obtain an exact mass distribution of ice fragments by collecting them without any melting loss as was experienced by Lange and Ahrens (1981) and Kawakami *et al.* (1983). This made it possible to compare with the distribution on rocks such as basalt and pyrophyllite (Fujiwara *et al.* 1977, Matsui *et al.* 1982, Takagi *et al.* 1984).

(1) The largest fragment mass at various impact conditions. The experimental conditions and results are summarized in Table V. A normalized mass of the largest fragment, the ratio of the largest fragment mass m_L to the initial target mass M_T, as low as 0.001 was attained by using cubic ice targets with edges 5 to 10 cm long. Figure 11 shows the normalized mass of largest fragment as a function of the energy density or the specific kinetic energy, the projectile kinetic energy E_k divided by the initial target mass. Comparing with the previous study of Kawakami *et al.* (1983), there exists the deviation larger than one order of magnitude in the present result, while the present one is generally consistent with the data from Lange and Ahrens (1981) and Cintala *et al.* (1985). This fact implies the employment of a "soft" ice target of 265 K in Kawakami *et al.* (1983). This deviation is not attributed to the size effect, although they used targets ranging in size from 10.5 to 30 cm. Lange and Ahrens (1981) impacted targets of 19 cm, two or four times as large as ours. The reason why the ice of Kawakami *et al.* was soft has not been clarified yet. We also examined the projectile material dependence for the fragmentation using the projectiles of ice, aluminum, and polycarbonate. The dependence was found in the threshold value for fragmentation: 60 joules/kg for ice and polycarbonate projectiles and 30 joules/kg for the aluminum one. Lange and

TABLE V
Experimental Conditions and Results of Fragmentation of Ice

Run No.	V_i m/s	M_T g	E_k J	E_{LS} J	E_k/M_T J/kg	P_0 MPa	P_I	m_L/M_T
IF1F	150	630	19	424	30	240	1.07×10^{-2}	>0.99
IF2F	263	730	58	557	81	315	1.22×10^{-2}	0.83
IF3F	300	876	77	636	87	360	1.16×10^{-2}	0.35
IF4F	300	1105	77	636	69	360	9.20×10^{-3}	0.64
IF5F	329	1067	92	707	86	400	1.07×10^{-2}	0.27
IF6F	358	1072	109	769	108	435	1.15×10^{-2}	0.09
IF7F	370	795	116	795	146	450	1.60×10^{-2}	0.045
IC1F	300	994	77	636	77	360	1.03×10^{-2}	>0.99
IC2F	332	949	94	707	99	400	1.20×10^{-2}	0.72
IC3F	352	976	105	751	108	425	1.24×10^{-2}	0.11
IC4F	363	454	112	777	247	440	2.75×10^{-2}	0.047
IC5F	392	1061	131	857	123	485	1.30×10^{-2}	0.16
IC6F	542	992	250	919	252	520	1.49×10^{-2}	0.017
IC7F	565	850	271	945	319	535	1.78×10^{-2}	0.016
IC8F	605	1013	311	990	307	560	1.56×10^{-2}	0.053
IC9F	756	193	486	1166	2512	660	9.68×10^{-2}	0.0016
IC10F	792	118	533	1184	4503	670	1.61×10^{-1}	0.0030
IC11F	816	838	566	1219	675	690	2.33×10^{-2}	0.0064
IC12F	854	117	620	1307	5303	740	1.79×10^{-2}	0.0012
AC1F	82	923	16	371	17	210	6.15×10^{-3}	>0.99
AC2F	116	895	31	548	35	310	9.30×10^{-3}	0.94
AC3F	127	914	37	601	41	340	1.00×10^{-2}	0.88
AC4F	183	1014	84	671	83	380	1.01×10^{-2}	0.16
AC5F	236	1015	139	813	137	460	1.23×10^{-2}	0.12
AC6F	277	310	192	884	619	500	4.33×10^{-2}	0.010
AC7F	277	1000	192	884	192	500	1.34×10^{-2}	0.037
AC8F	389	959	378	1078	395	610	1.71×10^{-2}	0.020
AC9F	422	991	445	1149	449	650	1.77×10^{-2}	0.009
AC10F	473	994	559	1272	563	720	1.95×10^{-2}	0.004
PC1F	248	942	65	618	69	350	1.01×10^{-2}	0.76
PC2F	277	910	81	689	89	390	1.16×10^{-2}	0.44
PC3F	301	925	95	760	103	430	1.25×10^{-2}	0.31
PC4F	327	956	112	795	117	450	1.28×10^{-2}	0.34
PC5F	346	926	126	813	136	460	1.34×10^{-2}	0.12
PC6F	687	883	496	1369	562	775	2.38×10^{-2}	0.009

Symbols in run numbers indicate the materials of projectile and target; IF, ice and Ice F; IC, ice and Ice C; AC, aluminum and Ice C; PC, polycarbonate and Ice C.

Ahrens (1981) defined a cratering process as the initial stage of fragmentation. The difference of projectile materials commonly results in a difference of energy efficiencies in cratering and in the initiation process of disruption in the fragmentation. Fragmentation to the relative mass of 0.1 occurred in the narrow range of 80 to 120 joules/kg for the specific kinetic energy. In higher range of specific energy the ice targets were totally reduced to the relative mass of 0.001, in which the projectile material dependence was not evident. This figure also shows that the fragmentation of ice occurred at lower specific energy than for basalts and pyrophyllite by an order of magnitude. Unlike the case of basalts and pyrophyllite (Takagi *et al.* 1984), it is obviously impossible to fit the present data to a single regression line. The least squares fitting in the range from 0.1 to 0.001 relative mass gives a power-law exponent of −1.2, which is intermediate between previous studies for basalts (Fujiwara *et al.* 1977, Matsui *et al.* 1982, Takagi *et al.* 1984).

Mizutani *et al.* (1990) proposed the nondimensional impact stress (NDIS) P_I as a new scaling parameter applicable to the fragmentation phenomena, defined by

$$P_I = \left(\frac{M_P/\rho_P}{M_T/\rho_T}\right)\frac{P_0}{Y},$$

where M_P, ρ_P, M_T, and ρ_T are the mass and density of projectile and target, respectively, and P_0 and Y represent the impact peak pressure and the material strength of the

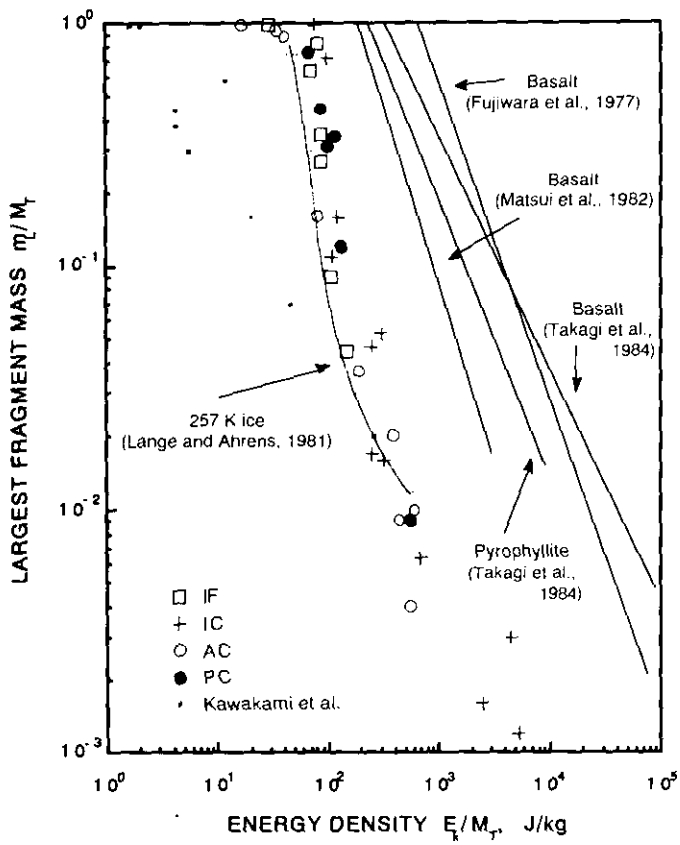

FIG. 11. Normalized mass of largest fragment versus energy density in ice, basalt, and pyrophyllite.

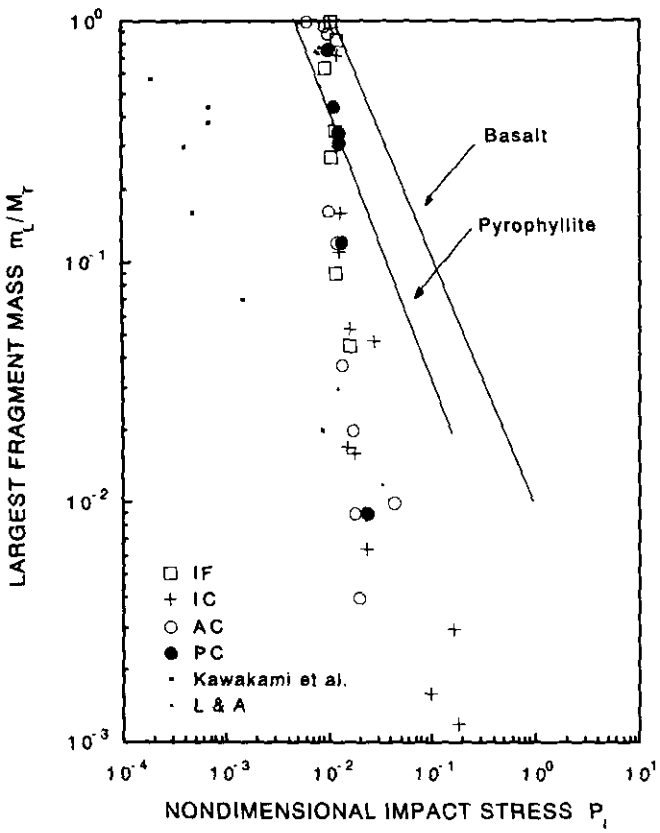

FIG. 12. Normalized mass of largest fragment versus nondimensional impact stress in ice, basalt, and pyrophyllite (Takagi *et al.* 1984).

target, respectively. Figure 12 represents the relation of relative largest fragment mass versus the P_I comparing with the previously studied results on basalts and pyrophyllite. Here, we adopted the dynamic compressive strength Y of 60 MPa for ice taking into account the strain rate variation, which was estimated from the maximum impact pressure of intact target. Similarly, we adopted dynamic strength of basalt (1.25 GPa) and pyrophyllite (980 MPa) from the compilation of Takagi *et al.* (1984). It was impossible to reexamine the data of Kawakami *et al.* (1983) for no record of impact conditions in which targets were kept intact. The initiation NDIS of fragmentation for ice can be plotted close to those for basalt and pyrophyllite. However, the value of slope is different, resulting in the large deviation between the ice and rocks in the advancing stage of disruption. In this plot it is impossible to fit the data by a single line of regression, as was the case in the plots of $\log m_L/M_T - \log E_k/M_T$. The relative mass of largest fragment abruptly decreased in a narrow range of P_I at a vicinity of 0.01, then the fragmentation progressed with a large slope. The impacts for small relative mass of largest fragment were carried out using small size of ice targets. It is possible to ascribe the descrepancy from the trend of large relative mass data to the size effect of material strength. Housen and Holsapple (1990) indicate the target size effect on material strength by $-3/8$ power of size. Following their theory data alignment is improved by 23% for the size difference of target size. However, no size effects were found between the Lange and Ahrens (1981) targets and our large targets $((6000/1000)^{1/3})$, although the size difference between them was the same as between two sizes of our targets $((1000/190)^{1/3})$. This study and the Lange and Ahrens result of 255 K ice showed that the fragmentation of ice initiated at the impact energy more than one order of magnitude larger than that of Kawakami *et al.* (1983). This difference is beyond size effect of material strength. It could plausibly result in the temperature effect on the ice strength.

In Fig. 12 we used the compressive strength of target material for calculating NDIS assuming the proportionality of compressive and tensile strength in the same manner as that of Takagi *et al.* (1984). By using the experimental tensile strength (17 MPa) of Lange and Ahrens (1983), neglecting the temperature difference of 240–245 K and 255 K of ours, ice data in Fig. 12 are shifted left by half an order of magnitude.

The size and temperature effects on material strength as well as the strain rate effect remain to be studied experimentally. They are very important to apply to the natural phenomena. For example, the transition size of planetary body from strength- to gravity-dominant fragmentation is largely dependent on tensile strength of constituting material (Housen *et al.* 1991).

(2) Mass distribution of ice fragments. A fragment mass of 10^{-5} g corresponds to the range of 10^{-7} to 10^{-8} of the initial target mass, which is more than four orders of magnitude smaller than in previous studies on ice. The cumulative mass distributions of fragments are presented in Figs. 13a to 13d, with each combination of projectile and target material. The data points at the smallest mass deviate from the trend of the other data. This is due to the underestimation of the average size of fragment passing through the largest number of sieve mesh. The total number of fragments was more than one order of magnitude larger than for basalts in the same NDIS and energy density. The dependence of the number of fragments on the impact energy is smaller than in the case of rocks; a difference of about one order of magnitude was observed for the energy density or NDIS at a normalized mass of 10^{-7}, although the difference of one order of magnitude was reported at a mass of 10^{-4} for the impact of basalt. Especially in the impact of ice to Ice C the difference was smaller in spite of factors of 20 for NDIS and 60 for energy density. These figures also indicate the dependence of the number of fragments on energy density or NDIS rather than on the impact velocity or the kinetic energy.

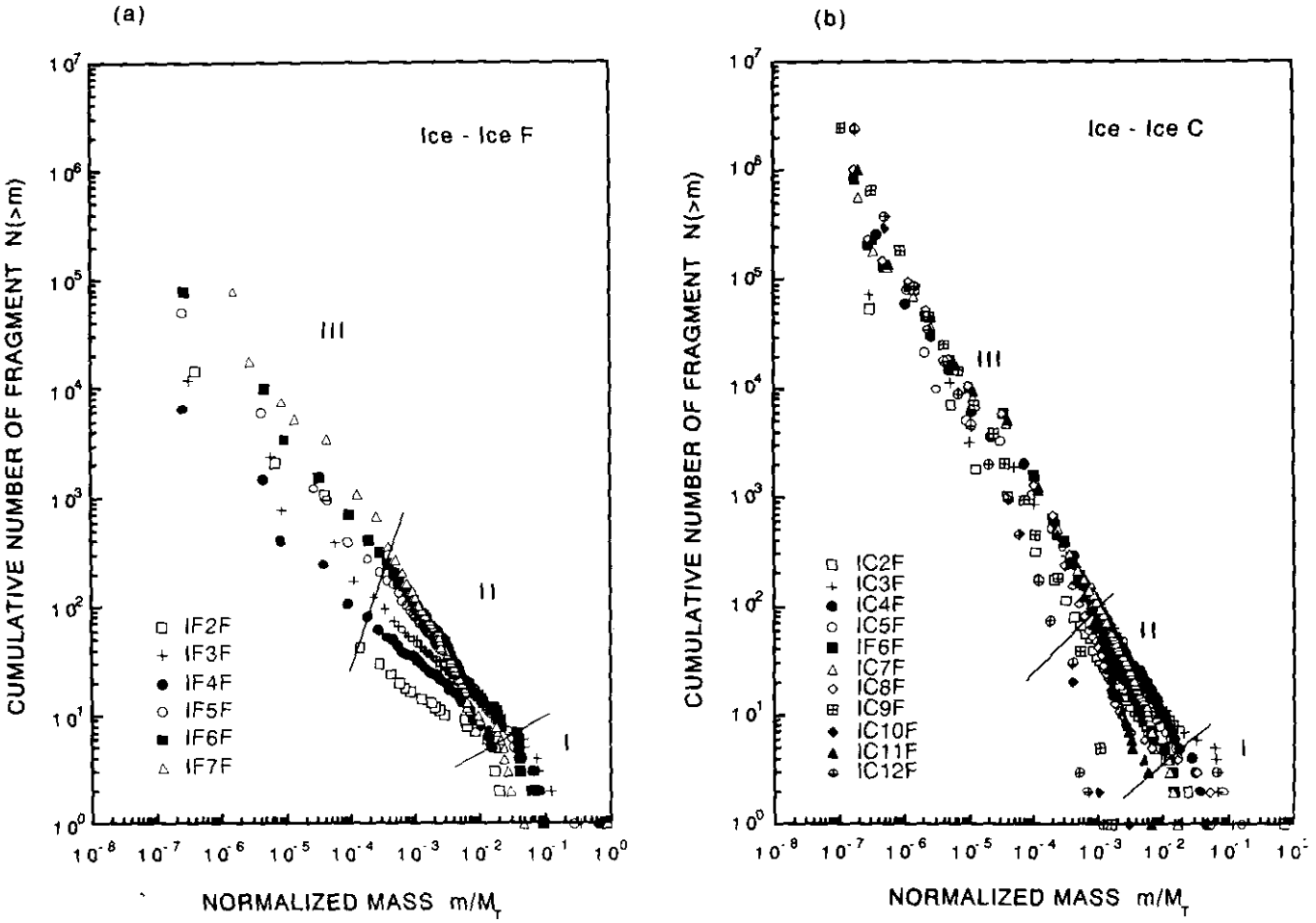

FIG. 13. Cumulative number versus normalized mass of fragments for four sets of projectile and target: (a) ice projectile to Ice F target, (b) ice to Ice C, (c) aluminum alloy to Ice C, and (d) polycarbonate to Ice C. Solid lines show the positions of the zone which the inflection points occupy.

Takagi *et al.* (1984) divided the mass distribution of basalt into three regions by two inflections in the same plotting as in Fig. 13. Inflections are also identified in these mass distributions of ice, but they are not clear unlike the case of basalt. The previous studies on the mass distribution by Lange and Ahrens (1981) and Kawakami *et al.* (1983) were limited in the regions of I and II. Our data expand to region III defined by the inflection around 10^{-4} relative mass. It is possible to estimate the power law constant in

$$N(>m) = Am^{-a}, \tag{1}$$

where $N(>m)$ gives the cumulative number of fragment heavier than m, and A and a are constants. The constant a, the value of slope of the region III, is summarized in the function of NDIS P_1 in Fig. 14. The slopes for the basalt and pyrophyllite by Takagi *et al.* (1984) are also presented to compare with the values for ice. The slope in region III for ice is almost constant at 0.7–0.9 in the range of $P_1 < 0.03$, which is significantly larger than for basalt and pyrophyllite of 0.4–0.6. In larger range of P_1 the slopes gently increase up to 1.3 in the same manner as for basalts.

We also collected the fragments ejected in the cratering experiments using semiinfinite targets to examine the mass distribution of fragments. Figure 15 shows the relation of cumulative number of cratering ejecta against ejecta mass in the cratering experiment. This figure indicates that the small fragments in the fragmentation experiment were formed by fracture in the vicinity of the impact point, because the total number of fragments, 10^6 to 10^7, and slope of region III in cratering, 0.8 to 1.3, are almost the same as the results in fragmentation using finite size of target.

We also plotted the relation of cumulative mass fraction $M(<D)$ with fragment size D, assuming the fragment to

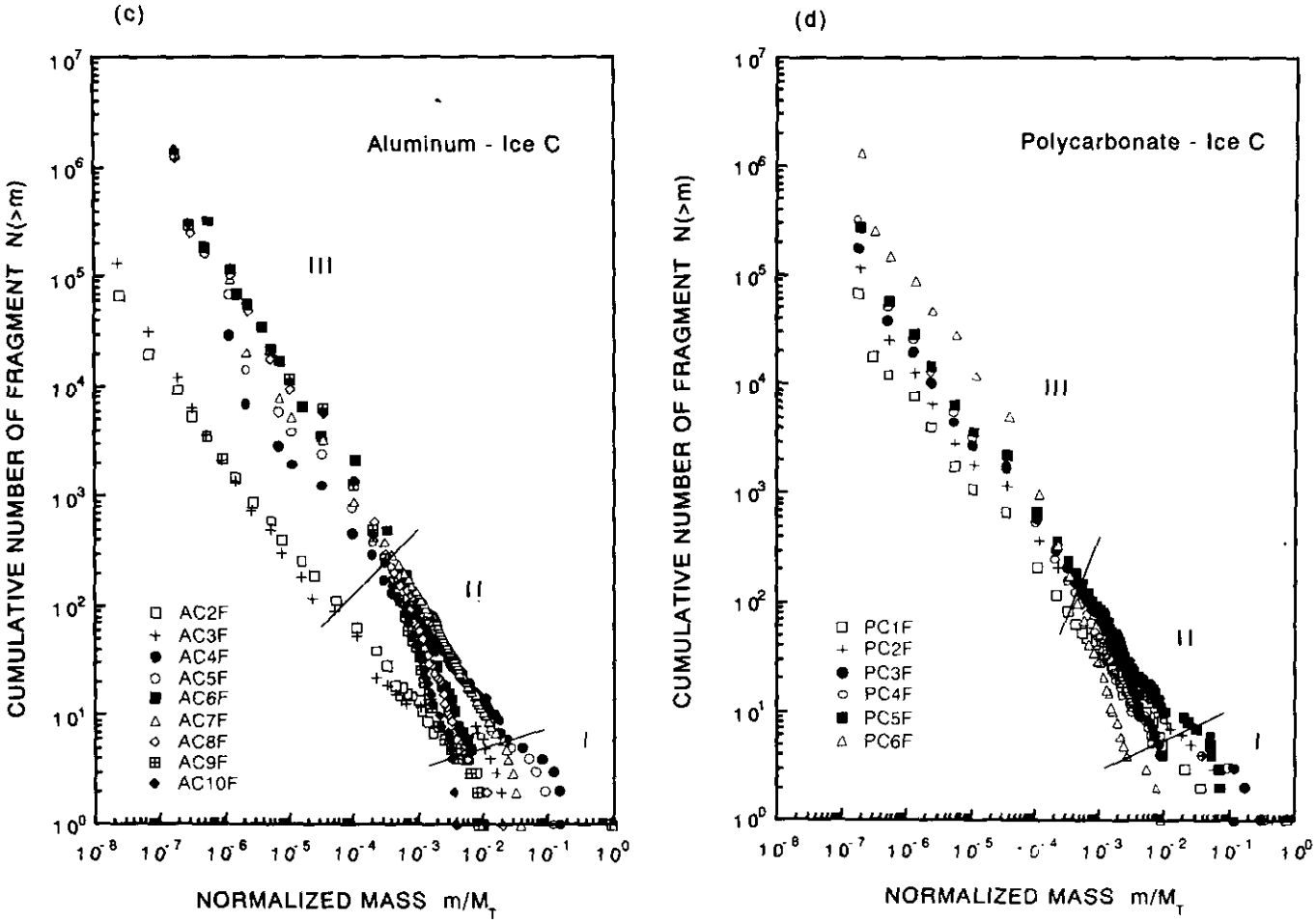

FIG. 13—*Continued*

be a sphere, to compare the previous results of basalt and other materials (Fujiwara *et al.* 1977; Grady and Kipp 1987). Figure 16 gives the result for the impact of ice to Ice C, which is very informative regarding the mass distribution of fragments. No significant inflections were found except for Runs IC2F, IC3F, and IC5F (with small NDIS) in contrast to the clear inflections in the basalt data of Fujiwara *et al.* (1977). The mass fraction data are so smooth that the curves can be fit by the following equation for Weibull representation of fragment (Grady and Kipp 1987),

$$M(<D) = 1 - \exp\left[-\left(\frac{D}{\sigma}\right)^n\right] \tag{2}$$

or for D sufficiently smaller than σ,

$$M(<D) = \left(\frac{D}{\sigma}\right)^n, \tag{3}$$

where σ is the scale parameter and power of n is the shape parameter. Least-squares fitting to Eq. (2) is very good in the larger range of NDIS and energy density; n is 0.79 ± 0.02 and σ is 0.026 ± 0.003 cm for Run IC12F.

Figure 16 also suggests that the fracture mechanism depends on the range of NDIS and energy density: multiple communication (Grady and Kipp 1987) at high NDIS and antipodal spallation to make large fragments at low NDIS.

When Eqs. (2) or (3) can be employed for the cumulative mass fraction, from the relation

$$M(<D) = \int_0^D M(D)n(D)\,dD, \tag{4}$$

differentiating Eq. (2), and replacing the fragment mass $M(D)$ of size D with D^3, we can get the size distribution density $n(D)$ in the following equation:

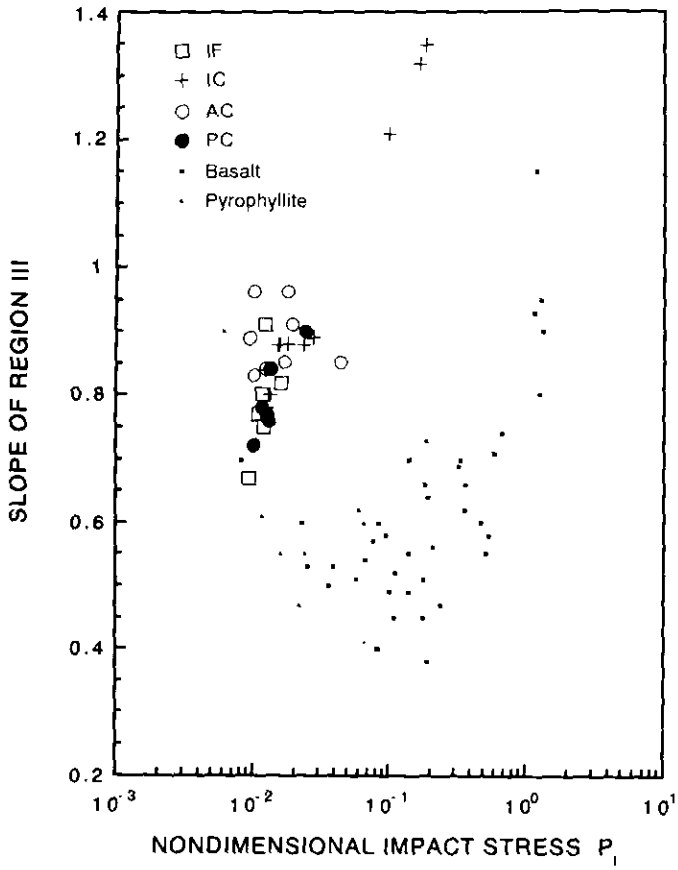

FIG. 14. Slope of region III versus nondimensional impact stress in mass distribution of fragments. The data for basalt and pyrophyllite are referred from Takagi *et al.* (1984).

$$n(D) \propto D^{-3}\left(\frac{D}{\sigma}\right)^{n-1} \exp\left[-\left(\frac{D}{\sigma}\right)^{n}\right]. \tag{5}$$

Integrating Eq. (5), the cumulative number of fragment $N(>D)$ in the function size D can be presented as follows:

$$N(>D) = \int_D n(D)\,dD \propto \int_D D^{-3}\left(\frac{D}{\sigma}\right)^{n-1} \exp\left[-\left(\frac{D}{\sigma}\right)^{n}\right] dD. \tag{6}$$

A numerical integration of Eq. (6) with $n = 0.79$ and $\sigma = 0.026$ and the experimental results for Run IC12F are compared in Fig. 17. Considering that the data point for the smallest fragments measured for Run IC12F is overestimated as mentioned above, the calculated curve agrees well with experimental data points. This result implies the inadequate identification of region III in Run IC12F. We must employ a slope in the range of size below 10^{-2} cm rather than the data in 0.1 to 0.02 cm. Using the relation (2) or (3), we reestimate the slope a of region III in Eq. (1) as shown in Fig. 18, in which the slope is almost constant, 0.62–0.75, in the range of NDIS from 0.1 to 3.

In the range of fragment size sufficiently smaller than σ, size distribution density $n(D)$ can be approximated to

$$n(D) \propto D^{-3}\left(\frac{D}{\sigma}\right)^{n-1} \propto D^{n-4}, \tag{7}$$

which means the size distribution of small fragments obeys the power law of size D. Grady and Kipp (1980) proposed the continuum model of explosive fracture, in which they clearly represented the strain rate dependence of fracture stress and dominant size of fragment. They also deduced the fragment distribution $F(D)$ with maximum value of distribution,

$$F(D) = \frac{\pi m k D^3}{12 C_g}\left(t_f - \frac{D}{2C_g}\right)^{m-1} \dot{\varepsilon}_0^m \tag{8}$$

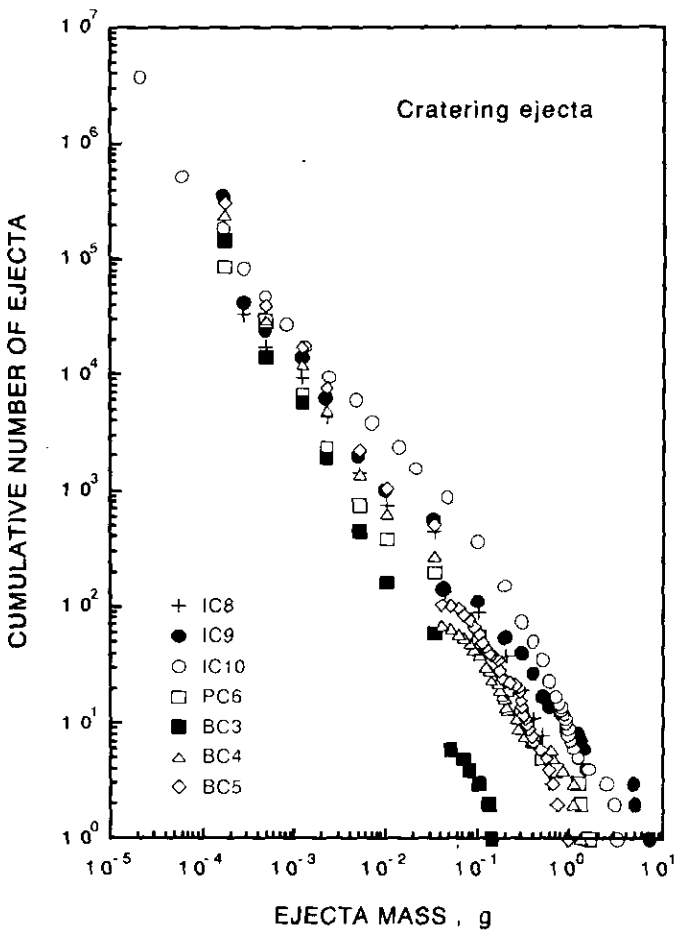

FIG. 15. Cumulative number versus ejecta mass in cratering experiments for seven runs.

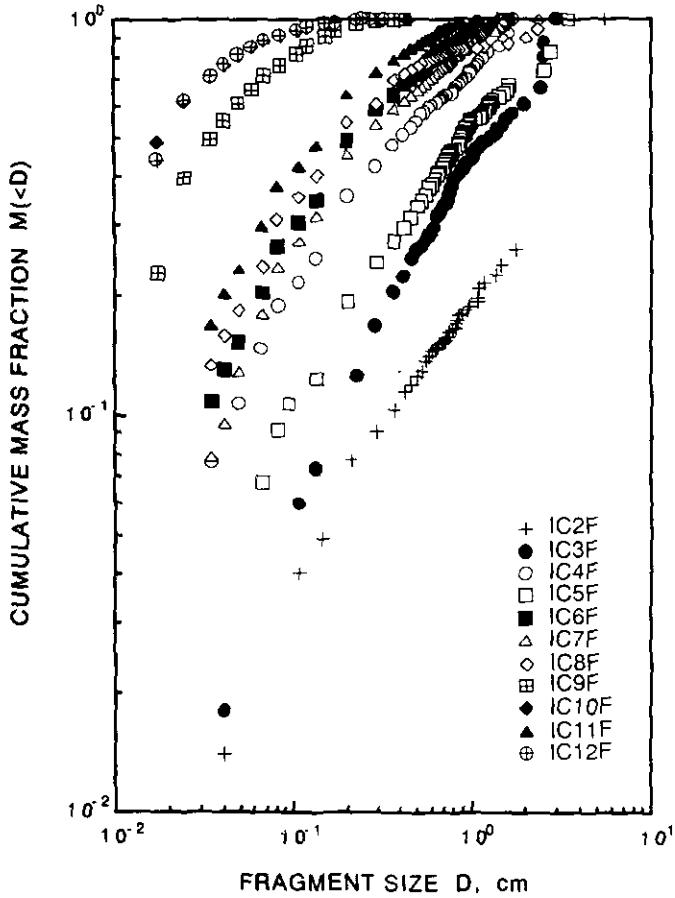

FIG. 16. Cumulative mass fraction $M(<D)$ versus fragment size D for the impact of ice to Ice C.

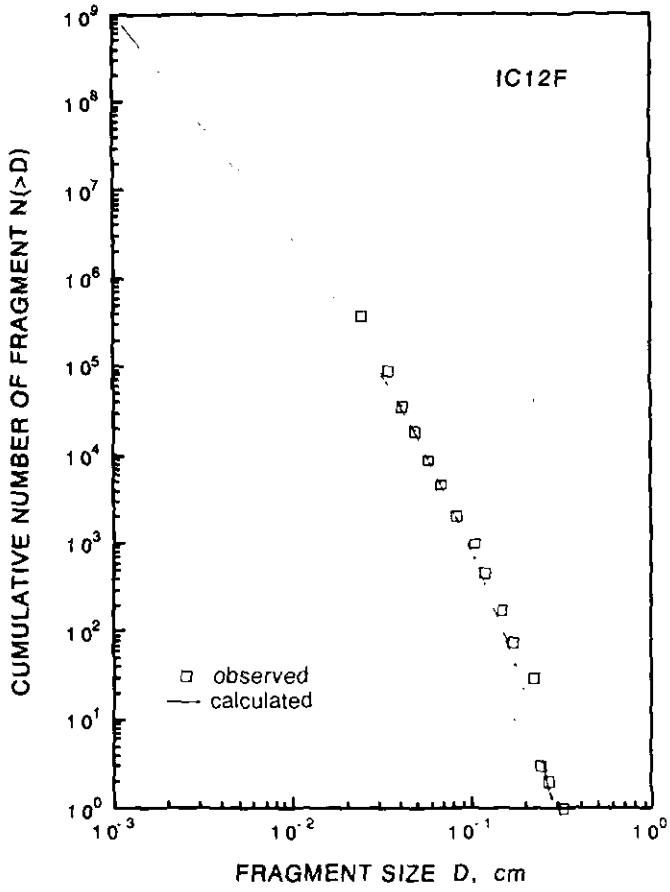

FIG. 17. Comparison of cumulative number versus fragment size with calculation used Eq. (6), n, and σ determined by least-squares fitting for Run IC12F.

where Cg and t_f are the fracture velocity and time, respectively, m and k are constants to be determined experimentally, and $\dot{\varepsilon}_0$ is the strain rate. Lange and Ahrens (1983) estimated m to be 8.3 from their experimental data of tensile strength, principal size of fragment, and the duration of tensile stress pulse. However, a slope of Eq. (8) was too steep to fit our data to the equation. We also tried to extend our sieve analysis to finer meshes to confirm the existence of small fragment cutoff, but we were unsuccessful because fine fragments smaller than 10^{-2} cm clogged the mesh. Microphotometry will be necessary to accurately determine the fragment size distribution down to less than 1 μm.

If the ice fragments were formed by multiple fracture processes following a power law of size D(a fractal structure) as shown in Eq. (7), we can compare our data with the natural size distribution of Saturn's ring. Kato *et al.* (1992) showed the constant power a of 0.8 to 0.9 for 77 K ice, slightly larger than that for our temperature of 255 K. From the microwave occultation on Saturn's ring by the spaceprobe Voyager (e.g., Tyler *et al.* 1983),

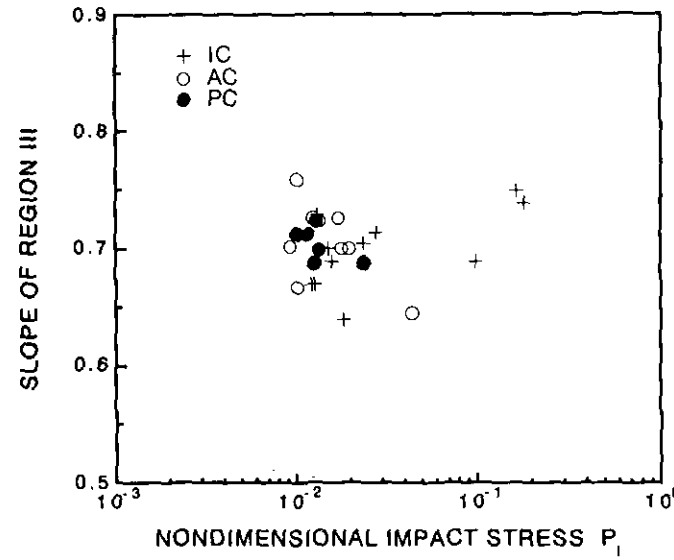

FIG. 18. Revised slope of region III versus nondimensional impact stress for group of Run IC, AC, and PC.

Marouf *et al.* (1983) estimated a power of -2.8 to -3.6 for the size distribution density of ring C in the range of grains smaller than 1 m. Using the relation

$$N(>D) = \int_D n(D)\, dD \propto D^{-(n-3)} \tag{9}$$

or

$$(n-3)/3 = -a \tag{9}$$

and our data of slope for 255 K and 77 K ice, we can lead to the power of -2.9 to -3.7 in Eq. (7). Because this agreement between the laboratory data and the estimates based on the observation of natural rings is too close to be fortuitous, we conclude that the formation of Saturn's ring was by collisional disruption.

CONCLUSIONS AND SUMMARY

We have presented data of ice impact using various scaling laws and representation schemes previously proposed on the basis of the experimental data for rocks such as basalt and pyrophyllite. The tests of applicability of previous studies to cratering and fragmentation of ice lead to the following conclusions. (1) The dependence of crater shape on the projectile material such as pit crater in ice to ice impacts was clearly observed; however, any scaling laws and theories have not elucidated it yet. (2) Although crater dimensions obeyed the power laws of E_k, E_{LS}, and π_3 in present impact conditions, the difference between using projectile materials has not yet been explained. (3) Inflections in variation trend of crater dimension also remain as a problem to be solved. (4) Fragmentation for ice initiated at the same range of NDIS as for rocks. This fact indicates the usefulness of NDIS as a scaling parameter. However, some modification such as selection of material strength Y are needed to apply the parameter in the progressing stage of fragmentation. (5) Size distributions of ice fragments follow exponential (Eq. (5)) or power laws (eq. (7)); however, theoretical background has not been made clear yet. An elucidation of fragmentation mechanism is required to construct the scaling law or theory for size distribution of impact fragments.

Although experimental results have not been theoretically accounted for yet, on the basis of our data it is possible to give some suggestions applying to the size distribution of Saturn's ring. In order to apply confidently the experimental data to natural events, and to make clear the temperature effect in impact processes we are progressing to ice impacts at low temperatures (77 K) by adding some technical improvements such as large target of 77 K ice for cratering and sieve analysis to smaller size of fragments.

ACKNOWLEDGMENTS

This study was made cooperatively by authors belonging to three institutes: Department of Earth and Planetary Sciences, Nagoya University; Institute of Low-Temperature Science, Hokkaido University; and Institute of Space and Astronautical Science. So many persons supported this work. We acknowledge Drs. H. Narita, Y. Mizuno, and K. Nishimura of ILTS for their technical advice and encouragements. We also appreciate greatly the technical help of T. Masuda and T. Torii of the Instrument Development Center of NU and T. Segawa and S. Nakatsubo of the Construction Division of ILTS. We also acknowledge Dr. E. S. Gaffney and Dr. S. K. Croft for their many useful suggestions on how to improve the manuscript. This study was supported by Grant-in-Aid for Scientific Research on Priority Areas (Origin of the Solar System) and (C) (No. 04835006) from the Ministry of Education, Science, and Culture, Japan.

REFERENCES

AHRENS, T. J., AND J. D. O'KEEFE 1985. Shock vaporization and accretion of the icy satellites of Jupiter and Saturn. In *Ice in the Solar System* (J. Klinger *et al.*, Eds.), pp. 631–654. Reidel, Dordrecht, Netherlands.

CINTALA, M. J., F. HÖRZ, S. SMREKAR, AND F. CARDENAS 1985. Impact experiments in H_2O ice. II. Collisional disruption. *Lunar Planet. Sci. XVI*, 129–130.

CROFT, S. K. 1981. Highpervelocity impact craters in icy media. *Lunar Planet. Sci. XII*, 190–192.

CROFT, S. K., S. W. KIEFFER, AND T. J. AHRENS 1979. Low-velocity impact craters in ice and ice-saturated sand with implications for martian crater count ages. *J. Geophys. Res.* **84,** 8023–8032.

FUJIWARA, A., G. KAMIMOTO, AND A. TSUKAMOTO 1977. Destruction of basaltic bodies by high-velocity impact. *Icarus* **31,** 277–288.

GAFFNEY, E. S. 1973. Study of the nature of shock waves in frozen Earth materials. *System Science and Software Report* SSS-R-73-1557, La Jolla.

GAFFNEY, E. S. 1985. Hugoniot of water ice. In *Ice in the Solar System* (J. Klinger *et al.*, Ed.), pp. 119–148. Reidel, Dordrecht, Netherlands.

GRADY, D. E., AND M.E. KIPP 1980. Continuum modelling of explosive fracture in oil shale. *Int. J. Rock Mech. Min. Sci. Geomech. Abstr.* **17,** 147–157.

GRADY, D. E., AND M. E. KIPP 1987. Dynamic rock fragmentation. In *Fracture Mechanics of Rock* (B. K. Atkinson, Ed.), pp. 429–475. Academic Press, London.

HARTMANN, W. K. 1969. Terrestrial, lunar, and interplanetary rock fragmentation. *Icarus* **10,** 201–213.

HOLSAPPLE, K. A., AND R. M. SCHMIDT 1982. On the scaling of crater dimensions 2. Impact processes. *J. Geophys. Res.* **87,** 1849–1870.

HOUSEN, K. R., AND K. A. HOLSAPPLE 1990. On the fragmentation of asteroids and planetary satellites. *Icarus* **84,** 226–253.

HOUSEN, K. R., R. M. SCHMIDT, AND K. A. HOLSAPPLE 1991. Laboratory simulation of large scale fragmentation events. *Icarus* **94,** 180–190.

KATO, M., Y. IIJIMA, Y. OKIMURA, M. ARAKAWA, N. MAENO, A. FUJIMURA, AND H. MIZUTANI 1992. Impact experiments on low temperature H_2O ice. In *Physics and Chemistry of Ice* (N. Maeno and T. Hondo, Ed.), pp. 237–244. Hokkaido Univ. Press, Sapporo.

KAWAKAMI, S., H. MIZUTANI, Y. TAKAGI, M. KATO, AND M. KUMAZAWA 1983. Impact experiments on ice. *J. Geophys. Res.* **88,** 5806–5814.

LANGE, M. A., AND T. J. AHRENS 1981. Fragmentation of ice by low velocity impact. *Proc. Lunar Planet. Sci.* **12B,** 1667–1687.

LANGE, M. A., AND T. J. AHRENS 1983. The dynamic tensile strength of ice and ice–silicate mixtures. *J. Geophys. Res.* **88,** 1197–1208.

LANGE, M., AND T. J. AHRENS 1987. Impact experiments in low-temperature ice. *Icarus* **69,** 506–518.

LARSON, D. B. 1984. Shock-wave studies of ice under uniaxial strain conditions. *J. Glaciol.* **30,** 235–240.

MAROUF, E. A., G. L. TYLER, H. A. ZEBKAR, R. A. SIMPSON, AND V. R. ESHLEMAN 1983. Particle size distributions in Saturn's rings from Voyager 1 radio occultation. *Icarus* **54,** 189–211.

MATSUI, T., T. WAZA, K. KANI, AND S. SUZUKI 1982. Laboratory simulation of planestesimal collisions. *J. Geophys. Res.* **87,** 10,968–10,982.

MELOSH, H. J. 1989. *Impact Cratering A Geologic Process.* Oxford Univ. Press, New York.

MIZUTANI, H., S. KAWAKAMI, Y. TAKAGI, M. KATO, AND M. KUMAZAWA 1983. Cratering experiments in sands and a trial for general scaling law. *J. Geophy. Res.* **88**(Suppl.), A835–A845.

MIZUTANI, H., Y. TAKAGI, AND S. KAWAKAMI 1990. New scaling laws on impact fragmentation. *Icarus* **87,** 307–326.

MOORE, H. J., D. E. GAULT, AND R. V. LUGN 1963. Experimental impact craters in basalt. *Trans. Min. Eng.* **229,** 258–262.

POLANSKEY, C. A., AND T. J. AHRENS 1990. Impact spallation experiments: Fracture patterns and spall velocities. *Icarus* **87,** 140–155.

SCHMIDT, R. M., AND K. R. HOUSEN 1987. Some recent advances in the scaling of impact and explosion cratering. *Int. J. Impact Eng.* **5,** 543–560.

TAKAGI, Y., S. KAWAKAMI, AND H. MIZUTANI 1984. Impact fragmentation experiments of basalts and pyrophyllites. *Icarus* **59,** 462–477.

TYLER, G. L., E. A. MAROUF, R. A. SIMPSON, H. A. ZEBKER, AND V. R. ESHLEMAN 1983. The microwave opacity of Saturn's rings at wavelengths of 3.6 and 13 cm from Voyager 1 radio occultation. *Icarus* **54,** 160–188.